Title: A methodology to determine 212Pb, 212Bi, 214Pb and 214Bi in atmospheric aerosols; Application to precisely obtain aerosol residence times and Rn-daughters' equilibrium factors

Authors: A. Barba-Lobo, I. Gutiérrez-Álvarez, E.G. San Miguel, J.P. Bolívar

Journal: Journal of Hazardous Materials, 445 (2023) 130521

DOI: https://doi.org/10.1016/j.jhazmat.2022.130521

A methodology to determine ^{212}Pb, ^{212}Bi, ^{214}Pb and ^{214}Bi in atmospheric aerosols; application to precisely obtain aerosol residence times and Rn-daughters' equilibrium factors

A. Barba-Lobo*, I. Gutiérrez-Álvarez, E.G. San Miguel, J.P. Bolívar

Radiation Physics and Environment Group (FRYMA), Department of Integrated Sciences, Center for Natural Resources, Health and Environment (RENSMA), University of Huelva, 21007, Huelva, Spain

ABSTRACT

Progeny of ^{222}Rn and ^{220}Rn, (^{212}Pb, ^{212}Bi, ^{214}Pb and ^{214}Bi) are essential to assess radiological hazard, external and internal doses, residence times and equilibrium factors. Precise measurements of these nuclides are quite complex due to their very short half-lives. This study outlines a new and precise methodology to measure these nuclides. Radon-222 and ^{220}Rn were measured using a radon monitoring system, while their respective progenies were collected in an atmospheric filter using an ASS-500 sampler and measured by gamma-ray spectrometry. The ^{212}Pb concentrations were very similar to the thoron ones, where all ^{212}Bi/^{212}Pb ratios were consistently less than 1. The relative uncertainties, σ_r, of the ^{212}Pb and ^{212}Bi activity concentrations, and ^{212}Bi/^{212}Pb activity ratio are generally less than 10%. Moreover, ^{214}Pb/^{222}Rn ratios were about 0.7, agreeing well with previous works. The σ_r for ^{214}Pb, ^{214}Bi and ^{214}Bi/^{214}Pb were generally less than 6%. This methodology was applied to estimate aerosol residence times using the ^{214}Pb/^{222}Rn and ^{212}Bi/^{212}Pb activity ratios, and to obtain equilibrium factors, achieving consistent results. Furthermore, the methodology consistency and validity range were studied with time elapsed between sampling end and counting start, and the sampling durations, finding the optimum times to precisely determine ^{212}Pb, ^{212}Bi, ^{214}Pb and ^{214}Bi.

Keywords: ^{220}Rn – ^{212}Pb – ^{212}Bi; ^{222}Rn – ^{214}Pb – ^{214}Bi; Aerosol residence times; Equilibrium factors; Gamma-ray spectrometry

*Corresponding author.
E-mail address: alejandro.barba@dci.uhu.es (A. Barba-Lobo)

1. Introduction

A fraction of ^{220}Rn (thoron, half-life, $T_{1/2}$ = 56 s), produced from radioactive decay of ^{224}Ra in the Earth's upper crust escapes the surface of the soils to the atmosphere. An assessment of inhalation dose from thoron requires a reliable method to measure ^{220}Rn concentration and its decay products in indoor and thus novel methods are being developed (Kanse et al., 2021). Among the radioactive progeny of thoron, ^{212}Pb has the longest half-life ($T_{1/2}$ = 10.6 h, Auranen and McCutchan, 2020), and thus allows to obtain detectable levels of this radionuclide in surface air. ^{212}Pb decays to ^{212}Bi ($T_{1/2}$ = 1.01 h). Due to its relatively long half-life, ^{212}Pb can be used as a tracer in environmental studies. In areas where ^{232}Th concentrations are higher in the upper crust, including soil at land-air interface, with higher background thoron concentration, special care needs to be taken to get reliable data of the decay products of ^{220}Rn for dose assessment (Balakrishnan et al., 2021; Haanes and Rudjord, 2018; Tokonami et al., 2004). Furthermore, recent findings have revealed that reassessment of risks due to radon exposure may need to take the presence of thoron and its progeny into account (Haanes and Rudjord, 2018; Tokonami, 2020).

It is well-known that radon (^{222}Rn, $T_{1/2}$= 3.82 d) and its progeny are the main source of ionization in the lower troposphere, due to its long half-life compared to ^{220}Rn and ^{219}Rn as well as the main natural source of equivalent dose to the public (Considine et al., 2005; Crawford et al., 2013; Crawford et al.,

2015; Zhang et al., 2011; Zhang et al., 2021). Radon is the second leading cause of lung cancer after smoking. Because the progeny of ^{222}Rn, ^{220}Rn and ^{219}Rn are highly particle-active and are charged at the time of their production, they are absorbed onto particulate matter present in air and hence ionizing radiation from particulate matter is a critical element in air quality. Inhaled particles could act as transport vehicles for radionuclides in their way inside the lungs, which may emit radiation after inhalation and deposition in the respiratory tract being able to damage the vascular structure (Macias-Verde et al., 2021; Pontedeiro et al., 2007; Yu et al., 2006) and also to affect different body organs (Gao et al., 2019). ^{214}Pb ($T_{1/2}$ = 26.8 min) and ^{214}Bi ($T_{1/2}$ = 19.9 min) are radon daughters that emit beta particles and many gamma rays with high branching ratios (e.g. 352 keV, 37.6%, and 609 keV, 46%) (DDEP, 2017; Ivanovich and Harmon, 1992). Lead-214 and ^{214}Bi have been used as tracers in several environmental applications. Examples include: i) as tracers to investigate the mixing of rain and seawater (Patiris et al., 2021); ii) to determine U concentrations in building materials and minerals (Kuzmanovic et al., 2021; Nuchdang et al., 2018; Pontedeiro et al., 2007) and iii) residence time estimation of cloud droplets and raindrops (Moriizumi et al., 2015).

The residence time calculated using the short-lived progeny of ^{222}Rn provides insights on how long it takes for atmospheric aerosol particles to settle to the ground in a specific area. Assuming steady-state between the production and removal rates, using a box model (Lozano et al., 2011), T_r can be estimated from the disequilibria between the parent and daughter nuclide. In the case of ^{238}U- and ^{232}Th-series radionuclides, the daughter nuclide is useful to determine the age when the half-life of the parent radionuclide is much larger than the daughter radionuclide. Consequently, for the case corresponding to ^{212}Bi/^{212}Pb, it is possible to use their ratio to obtain T_r. However, for the other case (^{214}Bi/^{214}Pb), it is not suitable given that their half-lives are very similar to each other. Therefore, for this latter case, it is necessary to select another ratio and ^{214}Pb/^{222}Rn is a possibility although the geochemical properties of Pb ad Rn are not similar.

In dosimetry, it is more convenient to characterize the short-lived progeny of radon through the potential alpha energy concentration (PAEC), which is the sum of the alpha particle decay energy of all the short-lived progeny of radon in a volume of air (J m^{-3}). Although originally defined for radon progeny, it is possible to extend it to include thoron progeny as well (Chalupnik et al., 2021). Other parameters often used to determine exposure and radiation dose by inhalation are the equilibrium-equivalent decay product concentration of airborne radon/thoron progeny and the equilibrium factor. The equilibrium-equivalent decay product concentration is the activity concentration of any radon/thoron daughter in equilibrium which leads to a determined value of the PAEC (Vargas et al., 2016). The equilibrium factor is defined as the ratio of the measured PAEC and the PAEC when all radon decay products are in secular equilibrium with ^{222}Rn (UNSCEAR, 2000).

For all the reasons previously mentioned, this study aims to develop a new methodology to determine ^{212}Pb, ^{212}Bi, ^{214}Pb and ^{214}Bi, as well as their ratios (^{212}Bi/^{212}Pb and ^{214}Bi/^{214}Pb) in atmospheric aerosols. Due to their low concentrations and short half-lives, precise measurements of these nuclides are complex. In comparison with other works related to the ^{212}Pb, ^{212}Bi, ^{214}Pb and ^{214}Bi determinations (e.g., Bem et al., 2002), our work is the first one to address these determinations by using an ASS-500 sampler, and a square filter whose dimensions are 44 cm x 44 cm. Furthermore, in our study, the obtained equations take into account the decay corrections in every moment, that is, during the sampling, between the sampling end and counting start, and during the counting, without needing to wait for the transient radioactive equilibrium. This makes our methodology more suitable to determine those radionuclides.

In addition, this study is the first one to address in-depth the determination of ^{212}Pb – ^{212}Bi and ^{214}Pb – ^{214}Bi outdoors. This methodology is applied to estimate the residence times of air aerosols, as well as to obtain the equilibrium factors for radon and thoron and their respective daughters which are essential for the internal dose calculation. For the estimation of aerosol residence times, the ^{214}Bi/^{222}Rn and ^{212}Bi/^{212}Pb activity ratios were employed, whereas this is the first study to use the ^{212}Bi/^{212}Pb ratio for the purpose previously mentioned. Furthermore, a comprehensive analysis is carried out on the optimum

sampling and counting times, and the times elapsed between the sampling start and counting end to minimize the uncertainties of the ^{212}Pb, ^{212}Bi, ^{214}Pb and ^{214}Bi activity concentrations, which has not been addressed in other studies.

2. Materials and methods

2.1. Materials and calibrations

All atmospheric sample collections took place at the El Carmen campus of Huelva University in Huelva (a province of Andalusia, Spain), whose geographical coordinates are 37º16´12´´N 6º55´28´´W. The sampling altitude was 6 m above the ground. Several polypropylene filters (44 cm x 44 cm) were selected for aerosol sample collection. Different air samples were collected using a high-volume aerosol sampler, model ASS-500 (details on ASS-500 sampler in Valkovic, 2000), which is able to reach air flows ranged from 500 m^3 h^{-1} to 600 m^3 h^{-1}. In Section 3.3, a comparison of the precisions determining the radionuclides of interest will be made between the ASS-500 and a PM_{10} samplers. In the case of the PM_{10} sampler, its filter holder was connected to an electronics system whose model was MCV – CAV-A/mb – High Volume Sampler, where the air flow of any PM_{10} sampler needs to be fixed at 68 m^3 h^{-1} according to the US EPA Compendium Method IO-2.1 (EPA, 1999).

Assay of ^{212}Pb, ^{212}Bi, ^{214}Pb and ^{214}Bi was conducted by gamma-ray spectrometry, using an extended energy range coaxial Ge detector (XtRa). The XtRa detector has a relative efficiency of 38.4% at 1332 keV (^{60}Co) (with respect to a 3"×3" NaI (Tl) detector), a full width at half maximum of 1.74 keV and 0.88 keV at 1332 keV and 122 keV, respectively, and a peak-to-Compton ratio of 67.5:1. The XtRa detector is connected to a device for the data acquisition and the gamma spectra visualization using the Genie 2000 software (Canberra Industries, 2004; Zhu et al., 2009). This detector was shielded with a Fe layer of 15 cm thickness, internally with a thin Pb layer. To avoid interferences from Pb X-ray in the obtained gamma spectra, a layer of 2 mm thick Cu plate was placed on the top of the Pb layer.

For the XtRa efficiency calibration, polypropylene 44 x 44 cm^2 filters were used for problem and calibration filters. A known amount of RGU-1 (4940(15) Bq kg^{-1}) and RGTh-1 (3250(45) Bq kg^{-1}) standards were well mixed between them and uniformly spread on three calibration filters, covering the same as that in sample collection. Then, they were subsequently folded achieving the same dimensions than the ones used for the measurements of any problem filter, that is, 11 x 11 cm^2. Three filters were chosen to check the reproducibility of the efficiency obtained for each selected energy. The detector was calibrated with the same radionuclides that are of interest in this study (^{214}Pb (352 keV), ^{214}Bi (609 keV), ^{212}Pb (238 keV) and ^{212}Bi (via ^{208}Tl (583 keV)). The true coincidence summing (TCS) correction was not considered since the radionuclides determined in the sample and calibration filters are identical, where both types of filters have the same geometry and dimensions and are measured at the same distance from the detector window, that is, just above the detector window to maximize the detector efficiency. For these reasons, the self-absorption effects were negligible (Barba-Lobo et al., 2021; Barba-Lobo and Bolívar, 2022). The quality control of the XtRa calibration for this type of filters was tested participating in several inter-comparison exercises organized by the Spanish Nuclear Safety Council (CSN), obtaining satisfactory results in all of them. The minimum detectable activities (*MDAs*) obtained for a counting time of 1 hour were 3 Bq, 8 Bq, 5 Bq and 7 Bq for the ^{212}Pb (238 keV), ^{212}Bi (583 keV), ^{214}Pb (352 keV) and ^{214}Bi (609 keV), respectively. For a sampling time of 1 hour and an air flow of 600 m^3 h^{-1}, *MDA* concentrations (*mda*) about 5 mBq m^{-3}, 13 mBq m^{-3}, 8 mBq m^{-3} and 12 mBq m^{-3}, respectively, were obtained.

The measured activity concentrations of ^{212}Pb, ^{214}Pb and ^{214}Bi were compared to their respective parents (thoron and radon), and the initial activities of ^{222}Rn and ^{220}Rn at the beginning of collection were measured. A measurement system, which was settled at the same place chosen to carry out the samplings, was utilized in order to determine the concentration levels of radon and thoron existing at

the beginning of each sampling. This system is based on Atmospheric Radon Monitoring (ARMON), which is comprised of a semiconductor detector inside a 20 L spherical detection volume, with a potential difference of 8000 V between sphere's the inner layer of the sphere and a Passivated Implanted Planar Silicon (PIPS) detector. In this system, the Si detector detects α-particles resulting from ^{216}Po and ^{218}Po decays, from the thoron and radon, respectively. The detector has a 1 μm filter which is placed at sphere entrance to trap all thoron and radon daughters, which are generated before entering this sphere. The *mda* were about 50 mBq m^{-3} and 200 mBq m^{-3} for thoron and radon, respectively. For further information about the ARMON system employed in this study and its calibration, see Vargas et al., 2015; Grossi et al., 2012. Regarding the quality control of the ARMON calibration, a chamber containing an active certified reference material is often measured by the ARMON and another system used for radon and thoron measurements (RAD7 version 5541, provided by DURRIDGE), which was already validated. For all these measurements carried out by the ARMON and RAD7, very similar curves of radon were obtained, validating the ARMON calibration.

Considering the previous materials mentioned, our experimental setup consisted of an ASS-500 aerosol sampler, using polypropylene filters of 44 x 44 cm^2, a XtRa Ge detector for the measurement of gamma-emitter radionuclides, and an ARMON for the measurement of radon and thoron.

2.2. Obtaining the equations related to the ^{212}Pb – ^{212}Bi and ^{214}Pb – ^{214}Bi determinations

In order to determine the activity concentrations of ^{212}Pb, ^{212}Bi, ^{214}Pb and ^{214}Bi in air at the beginning of the samplings, it is necessary to know precisely the activity of these radionuclides for the particulate matter deposited on the filters during the samplings, that is, A_{ps} (where p refers to the parent radionuclides, that is, ^{212}Pb or ^{214}Pb) and A_{ds} (where d refers to the daughter radionuclide, that is, ^{212}Bi or ^{214}Bi), can be obtained by the following equations (Supplementary Material-A for further information about the detailed demonstrations to obtain these equations and all the others shown in this Section):

$$A_{ps} = a_p \, \phi \, C_{ps} \tag{1}$$

where ϕ is the flow resulting from each sampling, $\Delta t_s = t_s^{(2)} - t_s^{(1)}$, where $t_s^{(1)}$ and $t_s^{(2)}$ are the times when each sampling starts and ends, respectively, $C_{ps} = \lambda_p^{-1}\left(1 - e^{-\lambda_p \Delta t_s}\right)$, λ_p is the decay constant of the parent radionuclide (that is, ^{212}Pb or ^{214}Pb) and a_p is the activity concentration of the parent radionuclide in air aerosol at $t_s^{(1)}$.

Then, using Bateman equation, the activity of A_{ds} is given as:

$$A_{ds} = \frac{a_p \, \phi \, \lambda_d}{\lambda_d - \lambda_p}\left[C_{ps} - C_{ds}\right] + a_d \, \phi \, C_{ds} \tag{2}$$

where λ_d and a_d are the decay constant and the activity concentration in air at $t_s^{(1)}$ of ^{212}Bi or ^{214}Bi, respectively, and $C_{ds} = \lambda_d^{-1}\left(1 - e^{-\lambda_d \Delta t_s}\right)$.

From Eqs. 1 and 2, the daughter/parent activity ratio can be determined which is useful to get information about the disequilibrium between the daughter and parent radionuclides referred to the particulate matter deposited during the sampling:

$$\frac{A_{ds}}{A_{ps}} = \frac{\lambda_d}{\lambda_d - \lambda_p} + \frac{C_{ds}}{C_{ps}}\left(\frac{a_d}{a_p} - \frac{\lambda_d}{\lambda_d - \lambda_p}\right) \tag{3}$$

The evolution of the activities of the parent and daughter radionuclides on the filters, and their ratios ($A_{ds}(t)/A_{ps}(t)$), at any time 't' can be known as follows:

$$A_{ps}(t) = A_{ps}\, C_{ps^{(2)}-t} \tag{4}$$

$$A_{ds}(t) = \frac{A_{ps}\,\lambda_d}{\lambda_d - \lambda_p}\left[C_{ps^{(2)}-t} - C_{ds^{(2)}-t}\right] + A_{ds}\, C_{ds^{(2)}-t} \tag{5}$$

$$\frac{A_{ds}(t)}{A_{ps}(t)} = \frac{\lambda_d}{\lambda_d - \lambda_p} + \frac{C_{ds^{(2)}-t}}{C_{ps^{(2)}-t}}\left(\frac{A_{ds}}{A_{ps}} - \frac{\lambda_d}{\lambda_d - \lambda_p}\right) \tag{6}$$

where A_{ps} and A_{ds} are given in Eqs. 1 and 2, respectively, $C_{ps^{(2)}-t} = e^{-\lambda_p\left(t-t_s^{(2)}\right)}$ and $C_{ds^{(2)}-t} = e^{-\lambda_d\left(t-t_s^{(2)}\right)}$.

After the sample collection, the filters were measured by a XtRa detector. Genie 2000 software was used to get the net counts (N) corresponding to each selected gamma energy of the radionuclides. N_p and N_d can be given by:

$$N_p = P_{\gamma p}\,\varepsilon_p\, A_{ps}\, C_{ps^{(2)}-c^{(1)}}\, C_{pc} \tag{7}$$

$$N_d = P_{\gamma d}\,\varepsilon_d\left\{\frac{A_{ps}\,\lambda_d}{\lambda_d - \lambda_p}\left[C_{ps^{(2)}-c^{(1)}}\, C_{pc} - C_{ds^{(2)}-c^{(1)}}\, C_{dc}\right] + A_{ds}\, C_{ds^{(2)}-c^{(1)}}\, C_{dc}\right\} \tag{8}$$

where P_γ and ε are the gamma emission probability and the efficiency for a given energy (p and d denote parent and daughter nuclides, respectively). $C_{ps^{(2)}-c^{(1)}} = e^{-\lambda_p\,\Delta t_{s^{(2)}-c^{(1)}}}$, $C_{ds^{(2)}-c^{(1)}} = e^{-\lambda_d\,\Delta t_{s^{(2)}-c^{(1)}}}$, $C_{pc} = \lambda_p^{-1}\left(1 - e^{-\lambda_p \Delta t_c}\right)$, $C_{dc} = \lambda_d^{-1}\left(1 - e^{-\lambda_d \Delta t_c}\right)$, $\Delta t_c = t_c^{(2)} - t_c^{(1)}$, being $t_c^{(1)}$ and $t_c^{(2)}$ the times corresponding to the start and end of the counting, respectively, and $\Delta t_{s^{(2)}-c^{(1)}} = t_c^{(1)} - t_s^{(2)}$.

Taking Eqs. 7 and 8, as well as Eqs. 1 and 2, the activity concentrations of the parent and daughter radionuclides in air, that is, at $t_s^{(1)}$, a_p and a_d, respectively, can be calculated as follows:

$$a_p = N_p\left[P_{\gamma p}\,\varepsilon_p\,\phi\, C_{ps}\, C_{ps^{(2)}-c^{(1)}}\, C_{pc}\right]^{-1} \tag{9}$$

$$a_d = \frac{1}{\phi\, C_{ds}}\left\{\frac{N_d\left(P_{\gamma d}\,\varepsilon_2\right)^{-1}}{C_{ds^{(2)}-c^{(1)}}\, C_{dc}} - \frac{N_p\left(P_{\gamma p}\,\varepsilon_p\right)^{-1}\lambda_d}{\lambda_d - \lambda_p}\left[\frac{1}{C_{ds^{(2)}-c^{(1)}}\, C_{dc}} - \frac{1}{C_{ps^{(2)}-c^{(1)}}\, C_{pc}}\right] - \frac{N_p\left(P_{\gamma p}\,\varepsilon_p\, C_{ps}\, C_{ps^{(2)}-c^{(1)}}\, C_{pc}\right)^{-1}\lambda_d}{\lambda_d - \lambda_p}\left[C_{ps} - C_{ds}\right]\right\} \tag{10}$$

Furthermore, using Eqs. 9 and 10, a_d/a_p is completely determined and, therefore, this ratio provides useful information about the disequilibria between the parent and daughter radionuclides at $t_s^{(1)}$:

$$\frac{a_d}{a_p} = \frac{"a_d"}{a_p} - \frac{\frac{C_{ps}\,\lambda_d}{\lambda_d - \lambda_p}\left[C_{ps^{(2)}-c^{(1)}}\,C_{pc} - C_{ds^{(2)}-c^{(1)}}\,C_{dc}\right]}{C_{ds}\,C_{ds^{(2)}-c^{(1)}}\,C_{dc}} - \frac{\lambda_d}{\lambda_d - \lambda_p}\left[\frac{C_{ps}}{C_{ds}} - 1\right] \quad (11)$$

where $"a_d" = N_d\left[P_{\gamma d}\,\varepsilon_d\,\phi\,C_{ds}\,C_{ds^{(2)}-c^{(1)}}\,C_{dc}\right]^{-1}$, that is, the activity concentration of the daughter radionuclide in the case that it did not have any dependence on the evolution of its parent activity concentration.

Considering Eqs. 9, 10 and 11, it is possible to know the uncertainties related to a_p, a_d and a_d/a_p:

$$\sigma(a_p) = a_p\frac{\sigma_{N_p}}{N_p} \quad (12)$$

$$\sigma(a_d) = \sqrt{(\beta+\gamma)^2\sigma_{N_p}^2 + \left(a_d + (\beta+\gamma)N_p\right)^2\left(\frac{\sigma_{N_d}}{N_d}\right)^2} \quad (13)$$

$$\sigma\left(\frac{a_d}{a_p}\right) = \frac{a_d}{a_p}\sqrt{\left(\frac{\sigma(a_p)}{a_p}\right)^2 + \left(\frac{\sigma(a_d)}{a_d}\right)^2} \quad (14)$$

where σ_{N_p} and σ_{N_d} are the uncertainties of N_p and N_d, respectively, $\frac{a_d+(\beta+\gamma)N_p}{N_d} = \frac{\partial a_d}{\partial N_d}$ and $\beta+\gamma = -\frac{\partial a_d}{\partial N_p}$.

For the samplings that will be carried out (see Sections from 3.1 to 3.5), the sampling time, Δt_s, was fixed at 0.5 h and 1.0 h, the time elapsed between the sampling end and the counting start, $\Delta t_{s^{(2)}-c^{(1)}}$, varied from about 0.3 h to 3 h, the counting time, Δt_c, was fixed at 0.5 h and 1.0 h, and the air flow varied from about 500 $m^3\ h^{-1}$ and 600 $m^3\ h^{-1}$. The counting and sampling strategy was stablished according to the half-life of the ^{212}Bi (1 hour), which is the radionuclide more difficult to measure considering its very short half-life and its relatively low concentration in air. So, the sampling and counting times were selected to be as short as possible to avoid significant decay of the analyzed radionuclides, and to minimize the uncertainties resulting when propagating uncertainties in the case of the activity concentrations in air.

2.2.1. Applications of the developed methodology: residence time and equilibrium factor estimations

From the disequilibrium between the daughter and parent radionuclides, the residence times of the atmospheric aerosols can be determined. Therefore, the methodology developed in this study in order to determine ^{212}Pb, ^{214}Pb, ^{212}Bi and ^{214}Bi was applied to the obtention of the residence times for air aerosols.

If between the two radionuclides selected to calculate those ratios, there is no intermediate decay products, T_r can be estimated by the following equation (Długosz-Lisiecka and Bem, 2012):

$$T_r = \frac{1}{\lambda_d(a_p/a_d - 1)} \quad (15)$$

where λ_d is the decay constant of the daughter radionuclide.

The uncertainty related to T_r can be calculated using:

$$\sigma(T_r) = \frac{1}{\lambda_d\left(1 - a_d/a_p\right)^2}\,\sigma(a_d/a_p) \tag{16}$$

where $\sigma(a_d/a_p)$ is the uncertainty related to a_d/a_p.

If there is an intermediate decay product, another equation is employed to estimate T_r (Robbins, 1978):

$$T_r = \left(\frac{-A + B}{2}\right)^{-1} \tag{17}$$

where $A = (\lambda_d + \lambda_{d'})$, $B = \sqrt{(\lambda_d + \lambda_{d'})^2 - 4\,\lambda_d\,\lambda_{d'}\,(1 - a_p/a_d)}$, λ_d and $\lambda_{d'}$ are the decay constants of the daughter radionuclide and the intermediate decay product, respectively. The uncertainty associated to Eq. 17 can be known as follows:

$$\sigma(T_r) = \frac{4\,\lambda_d\,\lambda_{d'}\,a_p/a_d^{\,2}}{B\,(-A + B)^2}\,\sigma(a_d/a_p) \tag{18}$$

Then, the methodology developed in this study was also employed to estimate the equilibrium factors of the radon and thoron daughters, F_{eq}, which are useful in order to get information about how significative the exposure to radiation is. In a general way, F_{eq} is defined as follows:

$$F_{eq} = C_{eq}/C_{Rn} \tag{19}$$

where C_{Rn} is the activity concentration of radon or thoron and C_{eq} is the equivalent activity concentration of the short-lived daughters of the radon or thoron, respectively, considering radioactive equilibrium between them. Therefore, depending on C_{eq} is referred to the radon or thoron daughters, this can be obtained by using one equation or another (Nader, 2019):

$$C_{eq}^{222} = 0.105\,a_{^{218}Po} + 0.515\,a_{^{214}Pb} + 0.380\,a_{^{214}Bi} \tag{20}$$

$$C_{eq}^{220} = 0.913\,a_{^{212}Pb} + 0.087\,a_{^{212}Bi} \tag{21}$$

where C_{eq}^{222} and C_{eq}^{220} are the equivalent activity concentrations when employing the daughters of the radon and thoron, respectively, and the activity concentrations of ^{218}Po, ^{214}Pb, ^{214}Bi, ^{212}Pb and ^{212}Bi in air. Besides, given that ^{218}Po is a very short-lived radionuclide (^{218}Po half-life ~ 3 minutes), it is very acceptable to assume secular equilibrium between ^{222}Rn and ^{218}Po.

3. Results and discussion

3.1. Determination of the ^{212}Pb, ^{214}Pb, ^{212}Bi and ^{214}Bi concentrations

Aerosol samplings of 1 hour of duration were carried out by using an ASS-500 sampler at "El Carmen" University Campus on July 22, 2021, starting at 5:00 UTC and finishing at 11:00 UTC.

The concentrations of ^{220}Rn and ^{212}Pb decrease since sunrise, that is, from about 6:00 UTC (Table 1). The ^{220}Rn concentration decreases from 509(163) mBq m^{-3} at 6:00 UTC to 105(75) mBq m^{-3} at 10:00 UTC. The corresponding values for ^{212}Pb decreased from 583(14) mBq m^{-3} at 6:00 UTC to 102(3) mBq m^{-3} at 10:00 UTC. Radon-222 and thoron usually reach their maximum concentrations at dawn, which took place between 5:00 UTC and 6:00 UTC on July 22, 2021. Furthermore, the ^{212}Pb values obtained at the beginning of sampling are statistically comparable with ^{220}Rn concentrations considering a significance level of 5%. Then, the ^{212}Bi/^{212}Pb activity ratio in all samples are less than 1 (Table 1), which is very consistent to the expected activity ratio values. The ^{212}Pb is the parent of the ^{212}Bi. Therefore, in the case that there is no excess accumulation, the ^{212}Bi/^{212}Pb activity ratio must be ≤ 1. Excess accumulation of the ^{212}Pb – ^{212}Bi happens rarely due to the high difference between their half-lives (10.6 hours (^{212}Pb) and 1 hour (^{212}Bi)). In addition, this reasoning can be corroborated by other works such as Bigu, 1993; He et al., 2017.

It is necessary to highlight the precision obtained for $a_{^{212}Pb}$, $a_{^{212}Bi}$ and $a_{^{212}Bi}/a_{^{212}Pb}$ using the methodology described in Section 2.2, with relative uncertainties ranged from 2.3% to 2.9%, from 7.8% to 11%, and from 8.3% to 12%, respectively. The $\Delta t_{s^{(2)}-c^{(1)}}$ values obtained for all samplings were relatively short, < 0.43 hours. This is essential to determine ^{212}Bi and ^{212}Pb and their activity ratios. Regarding the uncertainty in thoron activity, it is relatively high, due to its very short half-life.

Table 1

Flow (ϕ), activity concentrations of ^{212}Pb, ^{212}Bi and ^{220}Rn, ^{212}Bi/^{212}Pb activity ratio, duration of sampling (Δt_s) and counting (Δt_c) and time elapsed between collection end and counting start ($\Delta t_{s^{(2)}-c^{(1)}}$) for the samplings done on July 22, 2021 using an ASS-500 sampler.*

Filter code	ϕ (m^3 h^{-1})	Δt_s (h)	$\Delta t_{s^{(2)}-c^{(1)}}$ (h)	Δt_c (h)	^{212}Pb (mBq m^{-3})	^{212}Bi (mBq m^{-3})	$\frac{^{212}Bi}{^{212}Pb}$	^{220}Rn (mBq m^{-3})
A101	596	0.97(5:00 UTC)	0.35	0.94	510(12)	179(17)	0.35(0.03)	457(154)
A102	490	0.92(6:00 UTC)	0.42	0.94	583(14)	281(22)	0.48(0.04)	509(163)
A103	550	0.92(7:00 UTC)	0.43	0.94	384(9)	164(17)	0.43(0.04)	409(146)
A104	589	0.93(8:00 UTC)	0.40	0.94	331(8)	149(15)	0.45(0.05)	155(90)
A105	519	0.92(9:00 UTC)	0.43	0.94	215(6)	134(14)	0.62(0.07)	<50
A106	582	1.05(10:00 UTC)	0.25	1.00	102(3)	71(8)	0.69(0.08)	105(75)

(*) Numbers in parenthesis denotes uncertainty (1σ) associated with the data. Besides, for each Δt_s, the start times of each sampling are also specified in parenthesis.

For the ^{214}Pb – ^{214}Bi pair and ^{222}Rn (Table 2), all values obtained for $a_{^{214}Pb}$ were less than those for radon. The average activity ratio of $a_{^{214}Pb}/a_{^{222}Rn}$, was found to be 0.73(0.03), which agrees well with the values reported earlier in literature for meteorological conditions characterized by not very windy and non-rainy days, and a relative humidity about 50% (Chen and Harley, 2018; Pontedeiro et al., 2007). It is interesting to note that ^{214}Pb and radon followed the similar behavior, since their concentrations decreased from dawning. The activity concentrations of ^{214}Bi were in a good agreement with the expected ones. The $a_{^{214}Bi}/a_{^{214}Pb}$ ratios ranged from 0.41(0.02) to 0.59(0.03), which are significatively less than 1 and provide information on the factors and processes causing the disequilibria between ^{214}Pb and ^{214}Bi. The $a_{^{214}Bi}/a_{^{214}Pb}$ ratio did not show a significant variation as occurred for the $a_{^{214}Pb}/a_{^{222}Rn}$ ratio, which is consistent since they are associated to the same air aerosols.

The uncertainties of $a_{^{214}Pb}$, $a_{^{214}Bi}$ and $a_{^{214}Bi}/a_{^{214}Pb}$ ranged from 1.0% to 2.9%, from 3.9% to 6.3%, and from 4.9% to 6.5%, respectively. The relative uncertainties of $a_{^{214}Pb}$ were very similar to the ones obtained for $a_{^{212}Pb}$ (see Table 1), while relative uncertainties for $a_{^{214}Bi}$ were significatively smaller than the $a_{^{212}Bi}$ ones (see Table 1). This is coherent because the uncertainties related to a_d (activity concentration uncertainty of the daughter radionuclide, see Eq. 13) are inversely proportional to N_d. Since the net counts obtained for the full-energy peak used for ^{214}Bi (at 609 keV) were an order of magnitude higher than the N_d values associated to the full-energy peak used for ^{212}Bi (583 keV), it is reasonable that $\sigma(a_d)$ for ^{214}Bi is less than the ^{212}Bi one.

Table 2

Flow (ϕ), activity concentrations of ^{214}Pb, ^{214}Bi and ^{222}Rn, ^{214}Bi/^{214}Pb and ^{214}Pb/^{222}Rn activity ratios, duration of sampling (Δt_s) and counting (Δt_c) and time elapsed between collection end and counting start ($\Delta t_{s^{(2)}-c^{(1)}}$) for the samplings done on July 22, 2021 using an ASS-500 sampler.*

Filter code	ϕ ($m^3\ h^{-1}$)	Δt_s (h)	$\Delta t_{s^{(2)}-c^{(1)}}$ (h)	Δt_c (h)	^{214}Pb (Bq m^{-3})	^{214}Bi (Bq m^{-3})	$\frac{^{214}Bi}{^{214}Pb}$	^{222}Rn (Bq m^{-3})	$\frac{^{214}Pb}{^{222}Rn}$
A101	596	0.97(5:00 UTC)	0.35	0.94	19.2(0.4)	7.8(0.3)	0.41(0.02)	26.3(1.8)	0.73(0.05)
A102	490	0.92(6:00 UTC)	0.42	0.94	17.1(0.4)	9.6(0.4)	0.56(0.03)	22.8(1.6)	0.75(0.06)
A103	550	0.92(7:00 UTC)	0.43	0.94	14.7(0.3)	7.0(0.3)	0.48(0.03)	19.9(1.4)	0.74(0.06)
A104	589	0.93(8:00 UTC)	0.40	0.94	11.5(0.3)	5.5(0.3)	0.48(0.03)	15.9(1.2)	0.72(0.06)
A105	519	0.92(9:00 UTC)	0.43	0.94	10.5(0.3)	4.8(0.3)	0.46(0.03)	12.9(1.1)	0.81(0.07)

A106	582	1.05(10:00 UTC)	0.25	1.00	5.96(0.14)	3.54(0.16)	0.59(0.03)	10.0(0.9)	0.60(0.06)

(*) Numbers in parenthesis denotes uncertainty (1σ) associated with the data. Besides, for each Δt_s, the start times of each sampling are also specified in parenthesis.

Besides studying how significative the disequilibrium between ^{212}Pb and ^{212}Bi, and between ^{214}Pb and ^{214}Bi are in air aerosols using a_d/a_p, it is also interesting to know the evolution of both couples of radionuclides before and after ending the samplings. This is possible to be assessed making use of the Eqs. 3 (during sampling) and 6 (after sampling) and employing the same values for a_p, a_d and Δt_s than the ones obtained for each sampling. Therefore, it is possible to reproduce the theoretical behavior that A_{ds}/A_{ps} (activity ratios during sampling) and $A_{ds}(t)/A_{ps}(t)$ (activity ratios after sampling) would follow in the case of the ^{212}Pb – ^{212}Bi and ^{214}Pb – ^{214}Bi couples for the particulate matter deposited on the filters.

In Fig. S1 (see Supplementary Material-B), A_{ds}/A_{ps} and $A_{ds}(t)/A_{ps}(t)$ were plotted for each couple of radionuclides and for each of the six samplings, where the time intervals that start from the end of the samplings were fixed at 3 hours, covering a very wide time range to get a proper analysis of A_{ds}/A_{ps} and $A_{ds}(t)/A_{ps}(t)$ (1 hour during sampling + 3 hours after sampling). The A_{ds}/A_{ps} ratios obtained for ^{212}Pb – ^{212}Bi were less than 1 during sampling (Fig. S1). The $A_{ds}(t)/A_{ps}(t)$ ratios, they reached values higher than 1 when the total time was 4 hours. However, this is consistent because of the excess accumulation of the daughter radionuclides. This agrees well with other previous works (Katona et al., 2004; Moriizumi et al., 2015). For the ^{214}Pb – ^{214}Bi couple, the A_{ds}/A_{ps} ratios reached values > 1 hour, where the $A_{ds}(t)/A_{ps}(t)$ ratios were more than three times higher than 1 for a total time of 4 hours. For the ^{214}Pb – ^{214}Bi couple, the excess accumulation of the daughter radionuclides was more significant than the one obtained for ^{212}Pb – ^{212}Bi pair. This is reasonable because in ^{214}Pb – ^{214}Bi pair their half-lives are similar to each other and, consequently, the effect of excess accumulation can be produced more easily than the ^{212}Pb – ^{212}Bi pair.

3.2. Comparison of residence times using ^{212}Bi/^{212}Pb and ^{214}Pb/^{222}Rn activity ratios and estimation of equilibrium factors

The atmospheric aerosol residence times calculated for the samplings carried out on July 22, 2021 are shown in Table 3. Let us call T_r as T_r^{212} and T_r^{214} when making use of ^{212}Bi/^{212}Pb and ^{214}Pb/^{222}Rn, respectively, to estimate T_r. Furthermore, in Table 3, the equilibrium factors are also shown for the samplings that took place on July 22, 2021 in the case of the radon and thoron and their respective daughters using Eqs. 20 and 21, respectively.

Table 3

Residence times estimated using ^{212}Bi/^{212}Pb (T_r^{212}) and ^{214}Pb/^{222}Rn (T_r^{214}), and equilibrium factors for thoron daughters (F_{eq}^{220}), and for radon daughters (F_{eq}^{222}) for the samplings carried out on July 22, 2021*. Furthermore, z_{score} was calculated for each T_r couple obtained for each sampling, $z_{score}^{T_r}$**.

Filter code	T_r^{212} (h)	T_r^{214} (h)	$z_{score}^{T_r}$	F_{eq}^{220}	F_{eq}^{222}
A101	0.78(0.10)	2.0(0.6)	-2.0	1.1(0.3)	0.59(0.04)

A102	1.3(0.2)	2.2(0.6)	-1.4	1.1(0.4)	0.65(0.05)
A103	1.10(0.18)	2.1(0.6)	-1.6	0.9(0.3)	0.62(0.05)
A104	1.2(0.2)	1.9(0.5)	-1.3	2.0(1.2)	0.61(0.05)
A105	2.4(0.7)	3.2(1.5)	-0.5	-	0.67(0.06)
A106	3.2(1.2)	1.1(0.3)	1.7	1.0(0.7)	0.55(0.05)

(*) Numbers in parenthesis denotes uncertainty (1σ) associated with the data. (**) The $z_{score}^{T_r}$ obtained for each T_r couple was calculated comparing T_r^{212} with T_r^{214}, since T_r^{214} was determined by using a larger number of validated measurement systems (XtRa and ARMON).

The T_r^{212} and T_r^{214} ranged from ~ 0.8 hour to 3 hours (Table 3), which were statistically compatible to each other considering uncertainties at 2 sigma level, that is, for a confidence interval of 95% (significance level of 5%). This statistical compatibility can be checked by using the z_{score} calculated for each T_r^{212}-T_r^{214} couple, $z_{score}^{T_r}$, where all $|z_{score}^{T_r}|$ were found to be ≤ 2. This is consistent since both pairs are expected to yield similar values for T_r.

The equilibrium factors calculated using F_{eq}^{220} or F_{eq}^{222} were statistically compatible with ≤ 1 for all samples considering a confidence interval of 68% (uncertainties given at 1 sigma level), which agree well with those found in previous studies (Chen and Harley, 2018; Pontedeiro et al., 2007). This is consistent since the equivalent activity concentration related to ^{218}Po, ^{214}Pb and ^{214}Bi or to ^{212}Pb and ^{212}Bi must be less than or equal to the one related to the ^{222}Rn or ^{220}Rn, respectively.

3.3. Comparison of the ^{212}Pb, ^{214}Pb, ^{212}Bi and ^{214}Bi activity concentration precisions using an ASS-500 and PM_{10} samplers

A comparison between the $\sigma(a_p)$, $\sigma(a_d)$ and $\sigma(a_d/a_p)$ values (Eqs. 12, 13 and 14, respectively) resulted from using an ASS-500 and a PM_{10} samplers. This comparison allows us to know which sampler is more appropriate to achieve more precise calculations for a_p, a_d and a_d/a_p by employing the methodology developed in Section 2.2 For this, a_p and a_d and, therefore, a_d/a_p were assumed to be the same than the ones using a PM_{10} sampler. This is an acceptable assumption because in the zone where the samplings were carried out, there is a PM_{10} sampler settled very near of the ASS-500 sampler (< 2 meters of distance). It is necessary to clarify that only the ASS-500 sampler could be used for the samplings because there was only one gamma detector available to measure filters. Consequently, since ^{212}Pb, ^{212}Bi, ^{214}Pb and ^{214}Bi are radionuclides characterized by their short half-lives, only the ASS-500 sampler was employed. Taking the same a_p and a_d values, as well as the same values for Δt_s, $\Delta t_{s^{(2)}-c^{(1)}}$ and Δt_c for each of the six samplings, it is possible to calculate N_p and N_d using Eqs. 7 and 8, respectively, and, therefore, $\sigma(a_p)$, $\sigma(a_d)$ and $\sigma(a_d/a_p)$ can be determined making use of Eqs. 12, 13 and 14, respectively. In Figs. 1 and 2, this comparison is shown for ^{212}Pb – ^{212}Bi and ^{214}Pb – ^{214}Bi, respectively. Furthermore, this comparison is shown numerically as well in Tables S1 and S2 (in Supplementary Material-B), respectively.

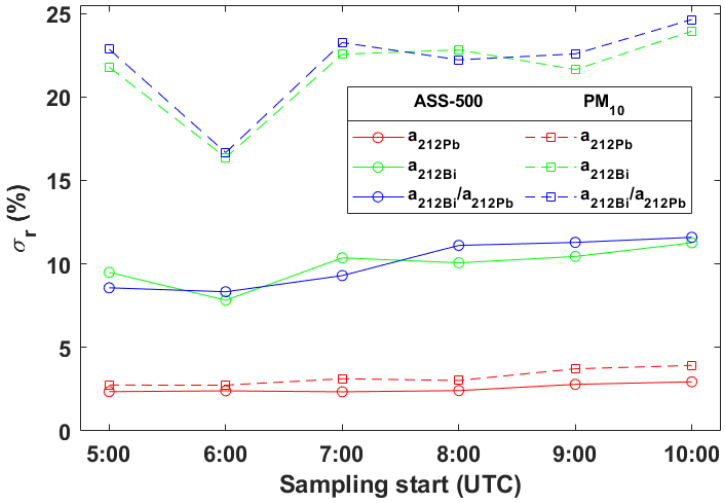

Fig. 1. Comparison of the precisions calculated the activity concentrations of the ^{212}Pb and ^{212}Bi, as well as for their ratios, in air using an ASS-500 and a PM_{10} samplers for the samplings carried out on July 22, 2021, where the relative uncertainties, σ_r (%), are plotted for each sampling start time.

As can be seen in Fig. 1, the relative uncertainties obtained for $a_{^{212}Pb}$ when using a PM_{10} sampler were somewhat higher than the ones achieved in the case of the ASS-500 sampler. However, for $a_{^{212}Bi}$ and $a_{^{212}Bi}/a_{^{212}Pb}$, the relative uncertainties were significatively higher than the ones obtained for the ASS-500 sampler (approximately two times higher). This is consistent since $\sigma(a_d)$ (see Eq. 13) is proportional to $\phi^{-1/2}$, where ϕ is the air flow reached by each sampler. Consequently, while ϕ for PM_{10} samplers needs to be fixed at 68 m^3 h^{-1} according to the US EPA Compendium Method IO-2.1 (EPA, 1999), the flow for ASS-500 samplers does not need to be fixed by the regulations, which can reach values ranging from 500 m^3 h^{-1} to 600 m^3 h^{-1}. This allows to sample a significantly higher volume of air, which is essential to determine ^{212}Bi in a much more precise way.

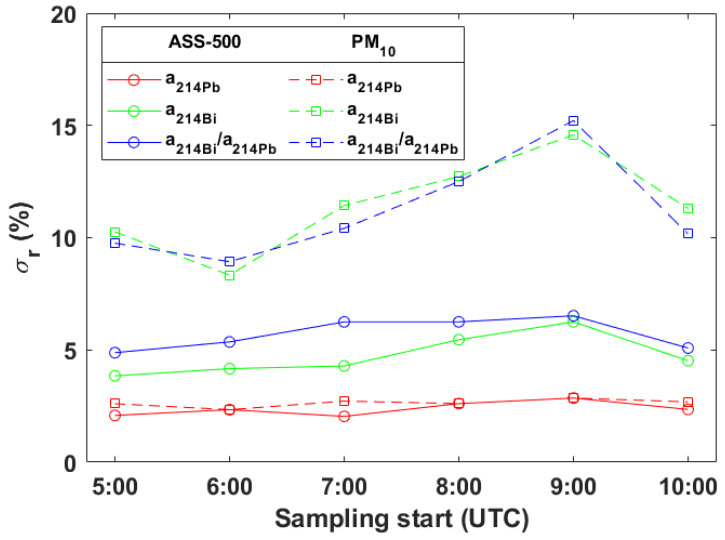

Fig. 2. Comparison of the precisions calculated the activity concentrations of the ^{214}Pb and ^{214}Bi, as well as for their ratios, in air using an ASS-500 and a PM_{10} samplers for the samplings carried out on July 22, 2021, where the relative uncertainties, σ_r (%), are plotted for each sampling start time.

For ^{214}Pb and ^{214}Bi (see Fig. 2), the relative uncertainties related to $a_{^{214}Pb}$ when using a PM_{10} sampler were similar to the ones previously obtained for the ASS-500 sampler. However, the precisions determining ^{214}Bi and ^{214}Bi/^{214}Pb were clearly worse for the PM_{10} sampler, getting relative uncertainties approximately two times higher than the ones resulting when using the ASS-500 sampler. This is consistent due to the same reason that was previously explained, that is, because of ϕ. Consequently, this proves that an ASS-500 sampler is much more suitable to be utilized to determine ^{212}Pb, ^{214}Pb, ^{212}Bi and ^{214}Bi.

3.4. Consistency and reproducibility of ^{212}Pb, ^{214}Pb, ^{212}Bi and ^{214}Bi activity concentrations and their ratios

The consistency and reproducibility of the methodology described in Section 2.2 was checked and its validity range was studied by estimating the total critical times ($\Delta t_s + \Delta t_{s^{(2)}-c^{(1)}} + \Delta t_c$), within which the ^{212}Pb, ^{214}Pb, ^{212}Bi and ^{214}Bi can be precisely determined. For this, two samplings were carried out using the ASS-500 sampler: first one on September 13, 2021, and the second one on September 15, 2021. For the first sampling, a Δt_s value of 1 hour was selected, and for the second one it was only 30 minutes, where for each sampling only one filter was used, which was measured six times in a row by the XtRa detector (30 minutes for each counting time).

The a_p, a_d and a_d/a_p of both couples of radionuclides were calculated for each measurement. Tables 4 and 5 show these concentrations for each $\Delta t_{s^{(2)}-c^{(1)}}$ value in the cases of the ^{212}Pb – ^{212}Bi and ^{214}Pb – ^{214}Bi, respectively, for the sampling carried out on September 13, 2021.

Table 4

Flow (ϕ), counting duration (Δt_c), activity concentrations of ^{212}Pb and ^{212}Bi and ^{212}Bi/^{212}Pb activity ratio for different $\Delta t_{s^{(2)}-c^{(1)}}$ values (1 hour-sampling, September 13, 2021). The activity concentration obtained for ^{220}Rn at 8:00 UTC was 473(159) mBq m^{-3}.*

Filter code	ϕ (m^3 h^{-1})	$\Delta t_{s^{(2)}-c^{(1)}}$ (h)	Δt_c (h)	^{212}Pb (mBq m^{-3})	$z_{score}^{^{212}Pb}$	^{212}Bi (mBq m^{-3})	$z_{score}^{^{212}Bi}$	$\frac{^{212}\text{Bi}}{^{212}\text{Pb}}$	$z_{score}^{^{212}Bi/^{212}Pb}$
A107	612	0.45	0.50	313(8)	-0.7	72(7)	0.2	0.23(0.02)	0.2
		0.98	0.50	320(8)	0.1	69(25)	0.0	0.22(0.08)	0.0
		1.50	0.50	324(8)	0.6	67(37)	-0.1	0.21(0.11)	-0.1
		2.00	0.50	317(8)	-0.2	-72(51)**	-	-	-
		2.52	0.50	325(8)	0.7	-180(74)**	-	-	-
		3.02	0.50	313(8)	-0.7	-322(102)**	-	-	-

	Average values	319(3)	0.5	69(15)	0.1	0.22(0.05)	0.1

(*) Numbers in parenthesis denotes uncertainty (1σ) associated with the data. (**) Activity concentrations not used in calculating average values, where z_{score} values are calculated with respect to the average values.

All $a_{^{212}Pb}$ were precisely calculated, getting relative uncertainties less than 2.6%, and all $a_{^{212}Pb}$ were statistically compatible with the one obtained for thoron (473(159) mBq m^{-3}) for a confidence interval of 68%, where the average a_{212Pb} was 319(3) mBq m^{-3}. Besides, all $|z_{score}^{^{212}Pb}|$ were less than 0.7, achieving an average $z_{score}^{^{212}Pb}$ of 0.5. Therefore, the consistence and reproducibility of the methodology developed in this study was good in the case of the ^{212}Pb. For the ^{212}Bi, it is possible to observe that the three first $a_{^{212}Bi}$ values agreed well with the average one (69(15) mBq m^{-3}), obtaining an average $z_{score}^{^{212}Bi}$ of 0.1, this same tendency being the one followed by the $a_{^{212}Bi}/a_{^{212}Pb}$ ratios, which further proves the good reproducibility of the methodology. Note that from the fourth counting, that is, the case corresponding to $\Delta t_{s^{(2)}-c^{(1)}}$ = 2 hours, $a_{^{212}Bi}$ started to be negative. This is consistent since 3.5 half-lives of the ^{212}Bi have been consumed and, consequently, the equation that provides $a_{^{212}Bi}$ (see Eq. 10) is not necessary because the ^{212}Bi is already following the same behavior that its parent, that is, they are in secular equilibrium. According to the results shown in Table 4 for $a_{^{212}Bi}$, it is possible to establish that the total time (Δt_s + $\Delta t_{s^{(2)}-c^{(1)}}$ + Δt_c) within which the ^{212}Bi determination can be precisely accomplished was approximately 2.5 hours.

Table 5

Flow (ϕ), counting duration (Δt_c), activity concentrations of ^{214}Pb and ^{214}Bi and ^{214}Bi/^{214}Pb activity ratio for different $\Delta t_{s^{(2)}-c^{(1)}}$ values (1 hour-sampling, September 13, 2021). The activity concentration obtained for ^{222}Rn at 8:00 UTC was 9.6(0.9) Bq m^{-3}.*

Filter code	ϕ (m^3 h^{-1})	$\Delta t_{s^{(2)}-c^{(1)}}$ (h)	Δt_c (h)	^{214}Pb (Bq m^{-3})	$z_{score}^{^{214}Pb}$	^{214}Bi (Bq m^{-3})	$z_{score}^{^{214}Bi}$	$\frac{^{214}\text{Bi}}{^{214}\text{Pb}}$	$z_{score}^{^{214}Bi/^{214}Pb}$
		0.45	0.50	7.71(0.18)	-1.4	3.2(0.3)	1.9	0.41(0.04)	1.7
		0.98	0.50	7.62(0.19)	-1.8	1.5(0.6)	-1.3	0.19(0.08)	-1.2
		1.50	0.50	7.9(0.2)	-0.6	-1.2(1.4)**	-	-	-
A107	612	2.00	0.50	7.8(0.3)	-0.7	-4(3)**	-	-	-
		2.52	0.50	8.1(0.4)	0.2	-15(6)**	-	-	-
		3.02	0.50	9.1(0.5)	2.0	-47(13)**	-	-	-
		Average values		8.03(0.13)	1.1	2.4(0.3)	1.6	0.30(0.05)	1.5

(*) Numbers in parenthesis denotes uncertainty (1σ) associated with the data. (**) Activity concentrations not used in calculating the average values, where z_{score} values are calculated with respect to the average values.

For the ^{214}Pb – ^{214}Bi (see Table 5), all $a_{^{214}Pb}$ were approximately 0.8 times the one obtained for radon (9.6(0.9) Bq m^{-3}). This is consistent with ^{214}Pb/^{222}Rn measurements previously shown in Section 3.1 (see Table 2). In addition, all $a_{^{214}Pb}$ were statistically comparable with the average one (8.03(0.13)) for a significance level of 5%, achieving an average $z_{score}^{^{214}Pb}$ of 1.1, demonstrating the good consistency and reproducibility of the methodology in the case of the ^{214}Pb. Then, for the ^{214}Bi, the two first values of $a_{^{214}Bi}$ shown in Table 5 agreed well with the average one (2.4(0.3) Bq m^{-3}), obtaining $|z_{score}^{^{214}Bi}|$ values less than 1.9, occurring the same for $z_{score}^{^{214}Bi/^{214}Pb}$. Note that $a_{^{214}Bi}$ started to be negative from a certain $\Delta t_{s^{(2)}-c^{(1)}}$ (1.50 hours), as previously occurred for the ^{212}Bi, which is reasonable because the total time consumed for $\Delta t_{s^{(2)}-c^{(1)}}$ = 1.50 hours was 3 hours. Consequently, the estimated total time within which ^{214}Bi can be determined in a proper way was approximately 2.5 hours.

With respect to the sampling carried out on September 15, 2021 whose duration was 0.5 hours, a study analogous to the previous one (sampling carried out on September 13, 2021) was done. In Tables S3 and S4 (see Supplementary Material-B), the results of a_p, a_d and a_d/a_p were shown for ^{212}Pb – ^{212}Bi and ^{214}Pb – ^{214}Bi, respectively, varying $\Delta t_{s^{(2)}-c^{(1)}}$ and fixing Δt_c at 0.5 hours. All $a_{^{212}Pb}$ were similar to each other, achieving an average $z_{score}^{^{212}Pb}$ of 0.7, and the $|z_{score}^{^{212}Bi}|$ values were less than 0.8 for positive $a_{^{212}Bi}$ (see Table S3). The $a_{^{212}Bi}$ values became negative when $\Delta t_{s^{(2)}-c^{(1)}} \approx 2$ hours, that is, for a total time of about 3 hours that is similar to the total critical time found for the previous sampling (September 13, 2021) which is consistent. For the ^{214}Pb and ^{214}Bi (see Table S4), all $a_{^{214}Pb}$ were statistically compatible with the average one (2.36(0.07) Bq m^{-3}) for a significance level of 5%. For the ^{214}Bi, the $z_{score}^{^{214}Bi}$ resulting from the first four measurements were less than 0.7. Therefore, the total time estimated to properly determine the ^{214}Bi was about 2 hours which agrees with the total time found for ^{214}Bi in the previous sampling (September 13, 2021), which further proves the consistency and reproducibility of the developed methodology.

The fact that $a_{^{212}Bi}$ and $a_{^{214}Bi}$ started to be negative from a certain total time can also be explained from a mathematical point of view. Rewriting Eq. 10 as $a_d = (\phi\, C_{ds})^{-1}\,(F_1 - F_2 - F_3)$, where $F_1 = \frac{\partial a_d}{\partial N_d}\, N_d\, \phi\, C_{ds} > 0$ and $-(F_2 + F_3) = \frac{\partial a_d}{\partial N_p}\, N_p\, \phi\, C_{ds} < 0$, it is possible to analyze the behavior of the F_i factors (i = 1, 2, 3), which are plotted in Figs. S2 and S3 (see Supplementary Material-B), having fixed Δt_c at 0.5 hours, and Δt_s at 1 hour and 0.5 hours (for samplings carried out on September 13, 2021 and September 15, 2021, respectively). As can be seen in Figs. S2 and S3 (Δt_s = 1 h and 0.5 h, respectively), the F_1 factor is much higher than F_2 and F_3 when $\Delta t_{s^{(2)}-c^{(1)}}$ tends to be zero for both cases (^{212}Bi and ^{214}Bi). However, as $\Delta t_{s^{(2)}-c^{(1)}}$ increases, F_2 and F_3 are gaining importance, especially for F_2. Consequently, at a certain $\Delta t_{s^{(2)}-c^{(1)}}$ value, F_2 + F_3 are higher than F_1 and, therefore, $a_{^{212}Bi}$ and $a_{^{214}Bi}$ become negative. This occurs when $\Delta t_{s^{(2)}-c^{(1)}}$ is about 2 and 1.5 hours for ^{212}Bi and ^{214}Bi, respectively (case for Δt_s = 1 h), which is consistent with the $\Delta t_{s^{(2)}-c^{(1)}}$ values found when Δt_s = 0.5 h, that are about 2 hours for ^{212}Bi and ^{214}Bi.

To complete the analysis about how the precision of the calculations for ^{212}Pb, ^{212}Bi, ^{214}Pb and ^{214}Bi, and their ratios depended on $\Delta t_{s^{(2)}-c^{(1)}}$, Δt_s as well as the concentrations in air, that is, a_i (i = p (parent) or d (daughter)), a theoretical study is shown below in the case of the relative uncertainties obtained for a_d/a_p considering different values of $\Delta t_{s^{(2)}-c^{(1)}}$, Δt_s and a_p when samplings are carried out using an ASS-500 sampler. Therefore, this analysis allows us to know the precision level by which is possible to calculate the disequilibrium existing between the parent and daughter for each couple of radionuclides.

3.5. Dependence of the a_d/a_p precision on varying $\Delta t_{s^{(2)}-c^{(1)}}$, Δt_s and a_p

An estimative analysis was performed on the precision (relative uncertainty, σ_r) by which is possible to determine the disequilibria between ^{212}Pb – ^{212}Bi and ^{214}Pb – ^{214}Bi. The σ_r values were plotted in Fig. 3 considering different C values, $C = a_d/a_p$, achieving to simulate several levels of disequilibrium, where C = 0.25 (high disequilibrium), C = 0.50 (medium disequilibrium) and C = 0.75 (low disequilibrium). Furthermore, the sampling duration, Δt_s, was fixed at 0.5 hours and 1 hour, the counting time, Δt_c, was fixed at 0.5 hours for all cases analyzed, and the time elapsed between the sampling end and the counting start, $\Delta t_{s^{(2)}-c^{(1)}}$, was ranged from 0.5 hours to 3 hours. Then, the activity concentration of the parent radionuclides, a_p, was fixed at 0.1, 0.2 and 0.3 Bq m^{-3} (for ^{212}Pb), and at 5, 12.5 and 20 Bq m^{-3} (for ^{214}Pb), covering the typical a_p values obtained for each radionuclide in the cases of low, medium and high concentration levels, respectively.

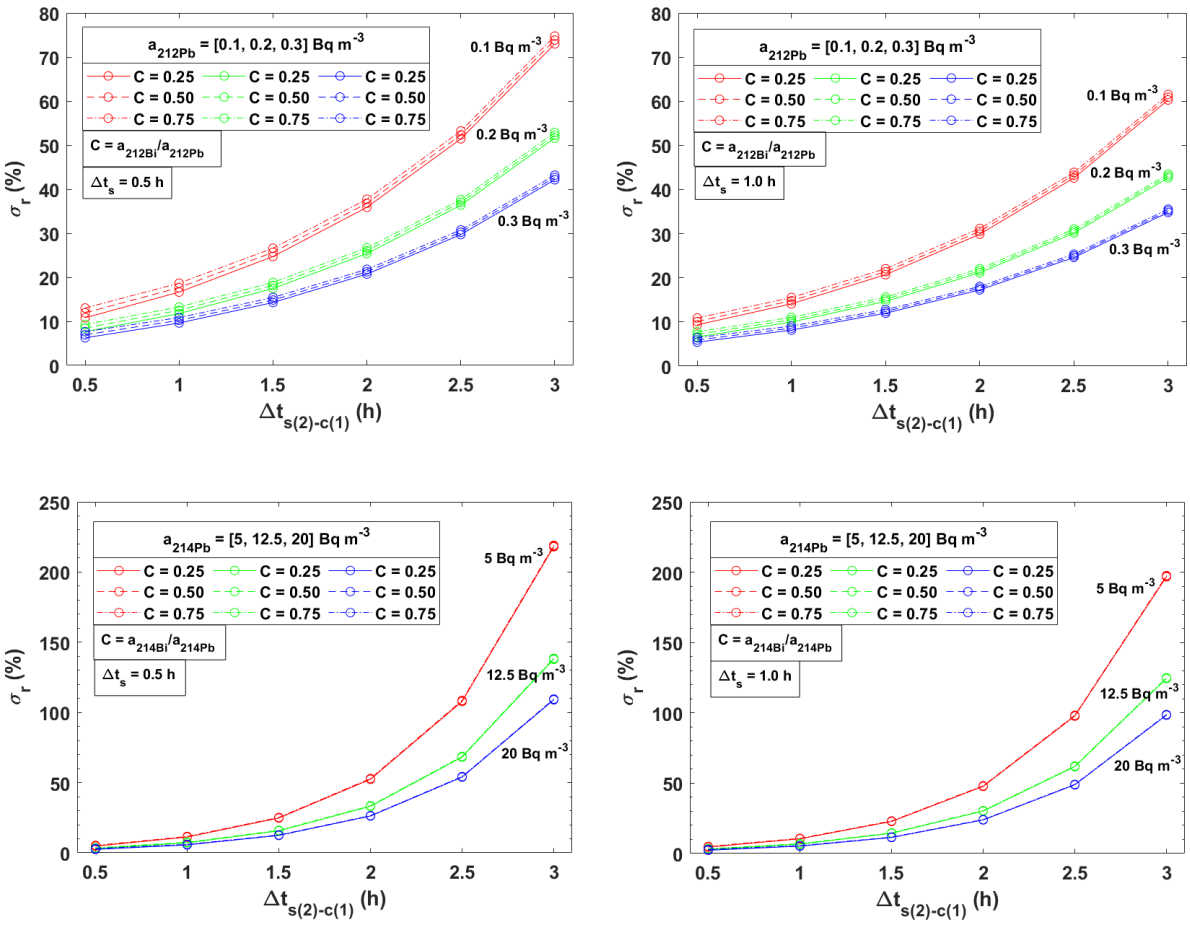

Fig. 3. Calculated relative uncertainties, σ_r (%), for several activity concentration ratios, C, of ^{212}Bi-^{212}Pb and ^{214}Bi-^{214}Pb. Counting times were fixed at 0.5 h and the time elapsed between the sampling end and the counting beginning, $\Delta t_{s^{(2)}-c^{(1)}}$, was varied from 0.5 h to 3 h (sampling time: 0.5 h and 1 h). The activity concentrations of the parent radionuclides in air, a_{212Pb} and a_{214Pb}, were fixed at 0.1, 0.2, 0.3 Bq m^{-3} and 5, 12.5, 20 Bq m^{-3}, respectively.

It is possible to observe that the σ_r dependence on a_p becomes stronger as $\Delta t_{s^{(2)}-c^{(1)}}$ increases. This is consistent with the σ_r behavior previously shown in Figs. 1 and 2 for a_d/a_p when using an ASS-500 sampler (see Section 3.3), where σ_r did not change significantly when varying a_p, since for the samplings analyzed in Section 3.3, $\Delta t_{s^{(2)}-c^{(1)}}$ was not a high value (~ 0.4 hours). The σ_r increases more quickly as $\Delta t_{s^{(2)}-c^{(1)}}$ increases in the case of the ^{214}Pb – ^{214}Bi compared to ^{212}Pb – ^{212}Bi. For Δt_s = 0.5 hours and $\Delta t_{s^{(2)}-c^{(1)}}$ = 2.5 hours, σ_r values ranged from 50% to 110% in the case of ^{214}Bi/^{214}Pb, while

for ^{212}Bi/^{212}Pb, the σ_r values ranged from 30% to 53%. Then, for Δt_s = 1 hour and $\Delta t_{s^{(2)}-c^{(1)}}$ = 2.5 hours, σ_r reached values ranged from 50% to 100% for ^{214}Bi/^{214}Pb, while for ^{212}Bi/^{212}Pb, the σ_r values ranged from 25% to 44%. Consequently, a good precision is more difficult to be achieved for the ^{214}Bi/^{214}Pb ratio, which is logical because the half-lives of ^{214}Pb and ^{214}Bi are much smaller than the ^{212}Pb and ^{212}Bi ones.

Note that for the same a_p value, σ_r has a weak dependence on *C* regardless of the selected $\Delta t_{s^{(2)}-c^{(1)}}$ value, which is especially true for the ^{214}Pb – ^{214}Bi couple. This means that the disequilibrium for each couple of radionuclides can be determined with the similar precision regardless of how significative that disequilibrium is. This agrees well with the behavior shown in Figs. 1 and 2, where σ_r was almost constant for all samplings studied.

Regarding the σ_r dependence on $\Delta t_{s^{(2)}-c^{(1)}}$, it is possible to observe that σ_r increases as $\Delta t_{s^{(2)}-c^{(1)}}$ increases for all cases considered, which is logical since as $\Delta t_{s^{(2)}-c^{(1)}}$ increases, more disintegrations of the radionuclides take place and, consequently, it is more complicated to get information of the disequilibria in a precise way. Furthermore, note that σ_r values are smaller when Δt_s = 1 hour than the ones obtained when Δt_s = 0.5 hours for the same value of $\Delta t_s + \Delta t_{s^{(2)}-c^{(1)}}$, but as shown in Section 3.4, as Δt_s increases, a_d becomes negative for shorter $\Delta t_{s^{(2)}-c^{(1)}}$ values. However, in Section 3.4, it has been demonstrated that the total times ($\Delta t_s + \Delta t_{s^{(2)}-c^{(1)}} + \Delta t_c$), within which the ^{212}Pb, ^{212}Bi, ^{214}Pb and ^{214}Bi, and their ratios can be determined, are very similar regardless of the selected Δt_s value, proving the consistency of the methodology developed in this study.

4. Conclusions

In the present study, a novel and precise methodology was developed to determine ^{212}Pb, ^{212}Bi, ^{214}Pb and ^{214}Bi contained in atmospheric aerosols using an ASS-500 sampler. The results obtained for the ^{212}Pb agreed well with the ones measured for ^{220}Rn. The activity concentrations for the ^{212}Bi were less than the ^{212}Pb ones. Regarding the ^{214}Pb – ^{214}Bi couple, the ^{214}Pb activity concentrations obtained in air were in good agreement with the measured ^{222}Rn, where the disequilibria found between ^{214}Bi and ^{214}Pb (between 0.5 and 0.7) agree with previous studies for similar meteorological conditions. All activity concentrations obtained for ^{214}Bi in air were less than ^{214}Pb ones, which is consistent with the expected behavior of them. The precisions obtained for ^{214}Pb and ^{214}Bi concentrations and their activity ratios in air were good.

The residence times were estimated using ^{212}Bi/^{212}Pb and ^{214}Pb/^{222}Rn ratios, obtaining statistically compatible residence times for each sampling, achieving all $|z_{score}| \leq 2$. All F_{eq} values achieved for both series (radon and thoron daughters) were consistent with the data reported in the literature, which all of them were statistically compatible with ≤ 1.

The precisions of the ^{212}Pb, ^{212}Bi, ^{214}Pb and ^{214}Bi determinations obtained when using an ASS-500 sampler were two times better than those obtained when using a PM_{10} sampler, which is due to the difference between their air flows.

For the tests of the consistency, reproducibility and validity range of the methodology, two samplings were carried out, whose durations (Δt_s) were 1 h and 0.5 h, respectively, and the counting durations (Δt_c) were fixed at 0.5 h. The time elapsed between sampling end and counting start, $\Delta t_{s^{(2)}-c^{(1)}}$, was varied verifying that all activity concentrations for each radionuclide were very similar to each other. The total times ($\Delta t_s + \Delta t_{s^{(2)}-c^{(1)}} + \Delta t_c$) within which ^{212}Bi and ^{214}Bi can be precisely determined were found to be 2 – 2.5 hours for Δt_s = 0.5 h and 1 h.

An analysis of the dependence of relative uncertainty, σ_r, on the ^{212}Pb and ^{214}Pb activity concentrations in air, Δt_s and $\Delta t_{s^{(2)}-c^{(1)}}$ was carried out for the ^{212}Bi/^{212}Pb and ^{214}Bi/^{214}Pb activity ratios. For specific ^{212}Pb and ^{214}Pb concentrations, almost the same values for σ_r were found regardless of the disequilibrium level between ^{212}Bi and ^{212}Pb, and between ^{214}Bi and ^{214}Pb. Furthermore, the σ_r values were smaller when Δt_s = 1 h than the ones obtained when Δt_s = 0.5 h for the same $\Delta t_s + \Delta t_{s^{(2)}-c^{(1)}}$ value. However, regardless of the selected Δt_s value, the estimated total times, within which the developed methodology provides relatively precise results, were very similar, which also verifies the good consistency and reproducibility of this methodology.

Acknowledgments

This research has partially funded by the projects of the Regional Government of Andalusia called "Treatment of acid leachates from phosphogypsum piles located at Huelva, and transport modelling of the released radionuclides" (Ref.: P20_00096), and "Valorization of inorganic wastes enriched in natural radioactivity for sustainable building materials" (Ref.: FEDER-UHU-202020), the project funded by the Spanish Nuclear Safety Council (CSN) "Radon exhalation from building materials; radiological impact and corrective measures" (Ref.: SUBV-4/2021), the project funded by the Spanish Ministry of Science, Innovation and Universities' Research Agency "Development and optimization of a process for removing natural radionuclides in phosphogypsum leachates" (Ref.: PID2020-116461RB-C21), and the Project for Novel Principal Investigators "Quantitative study of the variables involved in the radon exhalation rate for granular solids; application to rafts of granular solid phosphogypsum" (Ref.: UHUPJ-00005-632). The authors would like to thank M. Baskaran for the explanations provided during the research stay of A.B.L. in the Wayne State University of Detroit (USA).

Appendix A. Supplementary Data

Appendix B. Supplementary Data

References

Auranen, K., McCutchan, E.A., 2020. Nuclear Data Sheets for A=212. Nuclear Data Sheets 168, 117–267. https://doi.org/10.1016/j.nds.2020.09.002.

Balakrishnan, D., Jojo, P.J., Khandaker, M.U., 2021. Inhalation dose in the indoor environment of Eloor industrial area, Kerala, India. Radiat. Phys. Chem. 188, 109655. https://doi.org/10.1016/j.radphyschem.2021.109655.

Barba-Lobo, A., San Miguel, E.G., Lozano, R.L. Bolívar, J.P., 2021. A general methodology to determine natural radionuclides by well-type HPGe detectors, Measurement 181, 109561. https://doi.org/10.1016/j.measurement.2021.109561.

Barba-Lobo, A., Bolívar, J.P., 2022. A practical and general methodology for efficiency calibration of coaxial Ge detectors, Measurement 197, 111295. https://doi.org/10.1016/j.measurement.2022.111295.

Bem, H., Bem, E.M., Krzeminska, M., Ostrowska, M., 2002. Determination of radioactivity in air filters by alpha and gamma spectrometry. Nukleonika 47, 87-91. http://www.nukleonika.pl/www/back/full/vol47_2002/v47n2p087f.pdf.

Bigu, J., 1993. Thoron (^{220}Rn) progeny reduction by an air cleaner of the polarized media filter type. Nucl. Instrum. Methods. Phys. Res. A 325, 357-364. https://doi.org/10.1016/0168-9002(93)91038-O.

Canberra Industries, 2004. Genie 2000 Spectroscopy software: Customization tools, Printed in the United States of America.

http://depni.sinp.msu.ru/~hatta/canberra/Genie%202000%20Customization%20Tools%20Manual.pdf.

Chalupnik, S., Skubacz, K., Grygier, A., Nowak, S., 2021. Application of TLD devices for radon and thoron PAEC measurements in air is the concept of "total PAEC" useful? J. Environ. Radioact. 234, 106616. https://doi.org/10.1016/J.JENVRAD.2021.106616.

Chen, J., Harley, N.M., 2018. A Review of Indoor and Outdoor Radon Equilibrium Factors-part I: ^{222}Rn. Health Phys. 115, 490–499. https://doi.org/10.1097/hp.0000000000000909.

Considine, D.B., Bergmann, D.J., Liu, H., 2005. Sensitivity of Global Modeling Initiative chemistry and transport model simulations of radon-222 and lead-210 to input meteorological data. Atmos. Chem. Phys. 5, 3389–3406. https://doi.org/10.5194/acp-5-3389-2005.

Crawford, J., Zahorowski, W., Cohen, D.D., Chambers, S., Stelcer, E., Werczynski, S., 2013. Estimating the near-surface daily fine aerosol load using hourly Radon-222 observations. Atmos. Pollut. Res. 4, 1-13. https://doi.org/10.5094/APR.2013.001.

Crawford, J., Chambers, S., Kang, C.-H., Griffiths, A., Kim, W.-H., 2015. Analysis of a decade of Asian outflow of PM_{10} and TSP to Gosan, Korea; also incorporating Radon–222. Atmos. Pollut. Res. 6, 529-539. https://doi.org/10.5094/APR.2015.059.

Długosz-Lisiecka, M., Bem, H., 2012. Determination of the mean aerosol residence times in the atmosphere and additional ^{210}Po input on the base of simultaneous determination of ^{7}Be, ^{22}Na, ^{210}Pb, ^{210}Bi and ^{210}Po in urban air. J. Radioanal. Nucl. Chem. 293, 135–140. http://dx.doi.org/10.1007/s10967-012-1690-5.

EPA, 1999. Compendium of Methods for the Determination of Inorganic Compounds in Ambient Air. Compendium Method IO-2.1: SAMPLING OF AMBIENT AIR FOR TOTAL SUSPENDED PARTICULATE MATTER (SPM) AND PM10 USING HIGH VOLUME (HV) SAMPLER. https://www.epa.gov/sites/default/files/2015-07/documents/epa-io-2.1.pdf.

Gao, X., Koutrakis, P., Blomberg, A.J., Coull, B., Vokonas, P., Schwartz, J., Baccarelli, A.A., 2019. Short-term ambient particle radioactivity level and renal function in older men: Insight from the Normative Aging Study. Environ. Int. 131, 105018. https://doi.org/10.1016/J.ENVINT.2019.105018.

Grossi, C., Arnold, D., Adame, J.A., López-Coto, I., Bolívar, J.P., De La Morena, B.A., Vargas, A., 2012. Atmospheric 222Rn concentration and source term at El Arenosillo 100 m meteorological tower in southwest Spain. Radiat. Meas. 47, 149–162. https://doi.org/10.1016/j.radmeas.2011.11.006.

Haanes, H., Rudjord, A.L., 2018. Significance of seasonal outdoor releases of thoron from airflow through a point source during natural ventilation of a mine-complex in thorium-rich bedrock. Atmos. Pollut. Res. 9, 1000-1008. https://doi.org/10.1016/j.apr.2018.03.007.

He, Z., Xiao, D., Lv, L., Zhou, Q., Shan, J., Qiu, S., Wu, X., 2017. Controlling ^{212}Bi to ^{212}Pb activity concentration ratio in thoron chambers. J. Environ. Radioact. 178-179, 77-83. https://doi.org/10.1016/j.jenvrad.2017.07.011.

Ivanovich, M., Harmon, R., 1992. Uranium-series disequilibrium: applications to earth, marine, and environmental science, second ed. Clarendon Press, United Kingdom.

Kanse, S. D., Sahoo, B. K., Gaware, J. J., Sapra, B. K., 2021. A novel method based on ^{220}Rn (thoron) exhalation rate of indoor surfaces for robust estimates of ^{220}Rn concentration and equilibrium factor to compute inhalation dose. Chemosphere 267, 128908. https://doi.org/10.1016/j.chemosphere.2020.128908.

Katona, T., Kanyar, B., Jobbagy, V., Kavasi, N., Molnar, A., Imre, K., 2004. Determination of radon daughter activities of different aerosol fractions by gross-α and gross-β measurements. Proceedings of the 4th European conference on protection against radon at home and at work Conference programme and session presentations, (p. 377). https://inis.iaea.org/collection/NCLCollectionStore/_Public/36/010/36010933.pdf?r=1.

Kuzmanovic, P., Todorovic, N., Mrda, D., Forkapic, S., Filipovic, L., Miljevic, B., Hansman, J., Knezevic, J., 2021. The possibility of the phosphogypsum use in the production of brick: Radiological and structural characterization. J. Hazard. Mater. 413, 125343. https://doi.org/10.1016/j.jhazmat.2021.125343.

Lozano, R.L., San Miguel, E.G., Bolívar, J.P., 2011. Assessment of the influence of in situ ^{210}Bi in the calculation of in situ ^{210}Po in air aerosols: Implications on residence time calculations using ^{210}Po/^{210}Pb activity ratios. J. Geophys. Res. 116, D08206. https://doi.org/10.1029/2010JD014915.

Macias-Verde, D., Lara, P.C., Burgos-Burgos, J., 2021. Same pollution sources for climate change might be hyperactivating the NLRP3 inflammasome and exacerbating neuroinflammation and SARS mortality. Med. Hypotheses 146, 110396. https://doi.org/10.1016/J.MEHY.2020.110396.

Moriizumi, J., Kondo, D., Kojima, Y., Liu, H., Hirao, S., Yamazawa, H., 2015. ^{214}Bi/^{214}Pb radioactivity ratio in rainwater for residence time estimation of cloud droplets and raindrops. Radiat. Prot. Dosimetry 167, 55–58. https://doi.org/10.1093/rpd/ncv220.

Nader, A.F., 2019. The determination of equilibrium factor of radon and thoron using LR-115 type II detector in a selected area from Basra Governorate, Iraq. J. Phys.: Conf. Ser. 1258, 012032. https://iopscience.iop.org/article/10.1088/1742-6596/1258/1/012032/pdf.

Nuchdang, S., Injarean, U., Hirunanekmongkol, K., Timasart, N., Saksengwijit, A., Leelanupat, O., Rattanaphra, D., 2018. Studies on the possibility of determination of uranium and thorium concentration in the Thai monazite ore processing samples using gamma-ray spectrometry technique. J. Phys. 12071. https://doi.org/10.1088/1742-6596/1144/1/012071.

Patiris, D.L., Pensieri, S., Tsabaris, C., Bozzano, R., Androulakaki, E.G., Anagnostou, M.N., Alexakis, S., 2021. Rainfall Investigation by Means of Marine In Situ Gamma-ray Spectrometry in Ligurian Sea, Mediterranean Sea, Italy. J. Mar. Sci. Eng. 9, 903. https://doi.org/10.3390/jmse9080903.

Pontedeiro, E.M., Heilbron, P.F.L., Cotta, R.M., 2007. Assessment of the mineral industry NORM/TENORM disposal in hazardous landfills. J. Hazard. Mater. 139, 563-568. https://doi.org/10.1016/j.jhazmat.2006.02.063.

Robbins, J.A., 1978. Geochemical and geophysical applications of radioactive lead. In: J.O. Nriagu, (ed.), Biogeochemistry of Lead in the Environment, Elsevier Scientific, Amsterdam, 285–393.

The Decay Data Evaluation Project (DDEP), 2017. http://www.nucleide.org/DDEP_WG/DDEPdata.htm (accessed 25 October 2021).

Tokonami, S., Sun, Q., Akiba, S., Zhuo, W., Furukawa, M., Ishikawa, T., Hou, C., Zhang, S., Narazaki, Y., Ohji, B., Yonehara, H., Yamada, Y., 2004. Radon and thoron exposures for cave residents in Shanxi and Shaanxi provinces. Radiat. Res. 162, 390–396. https://doi.org/10.1667/RR3237.

Tokonami, S., 2020. Characteristics of thoron (^{220}Rn) and its progeny in the indoor environment. Int. J. Environ. Res. Public Health 17, 1–19. https://doi.org/10.3390/ijerph17238769.

UNSCEAR, 2000. SOURCES AND EFFECTS OF IONIZING RADIATION United Nations Scientific Committee on the Effects of Atomic Radiation: Vol. I (Issue c).

Valkovic, V., 2000. Radioactivity in the Environment: Physicochemical aspects and applications, first ed. Elsevier, Croatia.

Vargas, A., Arnold, D., Adame, J.A., Grossi, C., Hernández-Ceballos, M.A., Bolívar, J.P., 2015. Analysis of the vertical radon structure at the Spanish “El Arenosillo” tower station. J. Environ. Radioact. 139, 1–17. https://doi.org/10.1016/j.jenvrad.2014.09.018.

Vargas, C., Stabile, L., Cardellini, F., Morawska, L., Buonanno, G., 2016. Effect of indoor-generated airborne particles on radon progenydynamics. J. Hazard. Mater. 314, 155-163. https://doi.org/10.1016/j.jhazmat.2016.04.051.

Yu, K.N., Lau, B.M.F., Nikezic, D., 2006. Assessment of environmental radon hazard using human respiratory tract models. J. Hazard. Mater. 132, 98-110. https://doi.org/10.1016/j.jhazmat.2005.11.087.

Zhang, B., Liu, H., Crawford, J.H., Chen, G., Duncan, T., Chambers, S., Kang, C.-H., Williams, A.G., Zhang, K.,

Considine, D.B., Sulprizio, M.P., Yantosca, R.M., 2021. Simulation of radon-222 with the GEOS-Chem global model: emissions, seasonality, and convective transport. Atm. Chem. Phys. 21, 1861–1887. https://doi.org/10.5194/acp-21-1861-2021.

Zhang, K., Feichter, J., Kazil, J., Wan, H., Zhuo, W., Griffiths, A.D., Sartorius, H., Zahorowski, W., Ramonet, M., Schmidt, M., Yver, C., Neubert, R.E.M, Brunke, E.-G., 2011. Radon activity in the lower troposphere and its impact on ionization rate: a global estimate using different radon emissions. Atm. Chem. Phys. 11, 7817–7838. https://doi.org/10.5194/acp-11-7817-2011.

Zhu, H., Venkataraman, R., Mueller, W., Lamontagne, J., Bronson, F., Morris, K., Berlizov, A., 2009. X-ray true coincidence summing correction in Genie 2000. Appl. Radiat. Isot. 67, 696–700. https://doi.org/10.1016/j.apradiso.2009.01.013.